OPEN

Correspondence and
requests for materials
should be addressed to
G.T.F. (gtfei@issp.ac.
cn)

Fano resonance in anodic aluminum oxide based photonic crystals

Guo Liang Shang[1], Guang Tao Fei[1], Yao Zhang[1,2], Peng Yan[1], Shao Hui Xu[1], Hao Miao Ouyang[1] & Li De Zhang[1]

[1]Key Laboratory of Materials Physics and Anhui Key Laboratory of Nanomaterials and Nanostructures, Institute of Solid State Physics, Hefei Institutes of Physical Science, Chinese Academy of Sciences, P. O. Box 1129, Hefei, 230031, P. R. China, [2]Hefei National Laboratory for Physical Sciences at the Microscale, University of Science and Technology of China, Hefei, Anhui 230026, P. R. China.

Anodic aluminum oxide based photonic crystals with periodic porous structure have been prepared using voltage compensation method. The as-prepared sample showed an ultra-narrow photonic bandgap. Asymmetric line-shape profiles of the photonic bandgaps have been observed, which is attributed to Fano resonance between the photonic bandgap state of photonic crystal and continuum scattering state of porous structure. And the exhibited Fano resonance shows more clearly when the sample is saturated ethanol gas than air-filled. Further theoretical analysis by transfer matrix method verified these results. These findings provide a better understanding on the nature of photonic bandgaps of photonic crystals made up of porous materials, in which the porous structures not only exist as layers of effective-refractive-index material providing Bragg scattering, but also provide a continuum light scattering state to interact with Bragg scattering state to show an asymmetric line-shape profile.

F ano resonance[1] is a type of resonant scattering phenomenon resulted from interference of a continuum state and a discrete state, which will give rise to an asymmetric line-shape of the profile[2–6], and has been found in many fields of physics[6–12]. Fano resonance as one of the important scattering phenomena will play an important role in the future integrated optical systems in which scatterings from different factors coexist[5]. Photonic crystals (PCs)[13,14], as novel optical materials with different refractive index periodically stacked in space, can exhibit photonic bandgaps (PBGs) in which propagation of incident light is inhibited. Since PCs exhibit a wide range of application prospects, the study of Fano resonance in PCs has become of great importance and drawn many attentions[15–23]. Recently, M.V. Rybin et al.[24,25] observed Fano resonance owing to the interaction between continuum Mie scattering and a narrow Bragg Band in the PBG of the synthetic opal photonic crystals. I.V. Soboleva et al.[26] analyzed Fano resonances in 1D photonic crystals of ZrO_2/SiO_2 bilayers multilayer structures. S. Nojima et al.[27] used Fano resonances to elucidate the resonance nature of the localized defect states in photonic crystals. Furthermore, it was found that the asymmetry PBG profiles can be tuned by changing the effective dielectric constant of materials[24], light incident angle[28] and thickness of the PCs[26].

Anodic Aluminum Oxide (AAO) based PC is a kind of porous material containing alternative stacked stem channel layer and branched channel layer[29–33]. Strong light scattering caused by the porous structure of AAO could serve as a continuum state. Meanwhile, Bragg scattering caused by periodically layered structure in AAO can be regarded as a discrete state. So the interference may occur between these two states[5], in this case Fano asymmetry profile in the PBG of AAO based PC could be observed. However little information is available about Fano resonance in AAO based PC. Although the asymmetry profiles of PBGs have been reported[29–32], they are not regarded as the results of Fano resonance. Mostly, the asymmetry profile of PBG is attributed to inhomogeneous structure of the sample and the resulted superposition of multiple PCs. Therefore, preparation of photonic crystal with homogeneous structure is very necessary for the study of Fano resonance in AAO based PCs.

In this paper, we prepared the AAO based PC with narrow photonic bandgaps using compensation voltage oxidation mode[33,34], which effectively avoids the undesired asymmetry from tapered nanopores and resulted nonperiodicity. In this AAO based PC with narrow PBG, we observed Fano resonance phenomenon of which the origin can be determined as interference of the continuum light scattering state and discrete light scattering state.
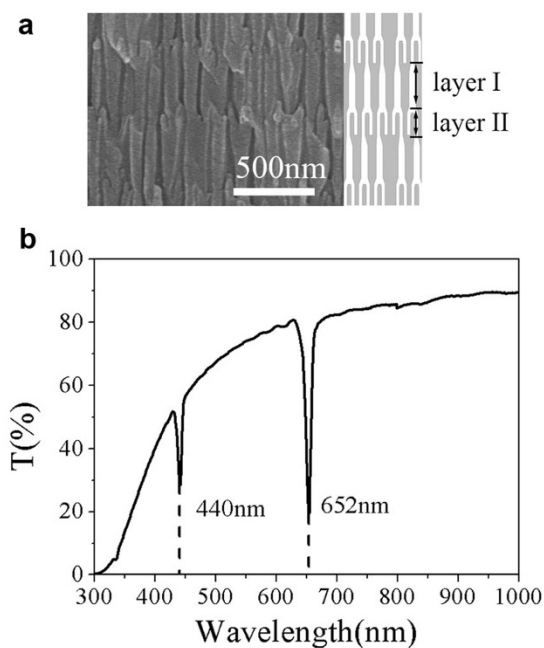
Figure 1 | SEM images and Transmittance of the as-prepared PC.
(a) Periodic structure of the AAO based PC (left), and schematic
illustration (right) in which the white part is air pore and the gray part is
alumina. (b) Transmittance spectrum of the as-prepared AAO based PC.

Results

Morphology and bandgap profile. Figure 1 shows the cross-
sectional SEM images and transmittance spectrum of the AAO
based PC. The as-prepared PC was about 47 μm thick (Figure 1a).
The periodic structure composes of alternately stacked stem channel
layers (layer I) and branched channel layers (layer II), leading to a
quasi-one dimensional PC along the pores growth direction. The
layered structure was schematic illustrated in the right side of
Figure 1a, in which the white part is air pore and the gray part is
alumina. The thicknesses of layer I and layer II are about 320 and
140 nm, and corresponding pore diameters are of 50 and 25 nm,
respectively.

Figure 1b is transmittance spectrum of the as-prepared sample,
which can be considered as two composing parts: One is the narrow
PBGs with centers located at 440 and 652 nm, respectively. The
corresponding full width at half maximum (FWHM) of the PBGs
are 8 and 10 nm, respectively. These ultra-narrow PBGs are bene-
fited from the uniform pore structure from beginning to end (see
Supplementary Figure S1) generated by the applied compensation
voltage mode during preparation which avoids the undesired asym-
metry from tapered nanopores and resulted nonperiodicity[33,34]. The
other is the continually decreased transmittance of the spectrum
(CDTS) with decreasing wavelength, which reduces to zero when
the wavelength is below 300 nm. Since AAO based PC is a kind of
porous material with the pore diameter is in nanometer order of
magnitude and thicknesses of stem and branched channel layers
are all around several hundred nanometers, the light scattering will
be stronger in shorter wavelength region, therefore, the transmit-
tance in shorter wavelength is much lower than that in longer
wavelength.

This narrow PBG will be great beneficial to demonstrate various
physical phenomena resulted from different factors in PCs.
Generally, PBG of an ideal PC exhibits a symmetry profile if only
strong Bragg scattering is considered. However, owing to the exist-
ence of light scattering from porous structure, interference between
this CDTS and Bragg scattering might occur[5], a Fano type profile of
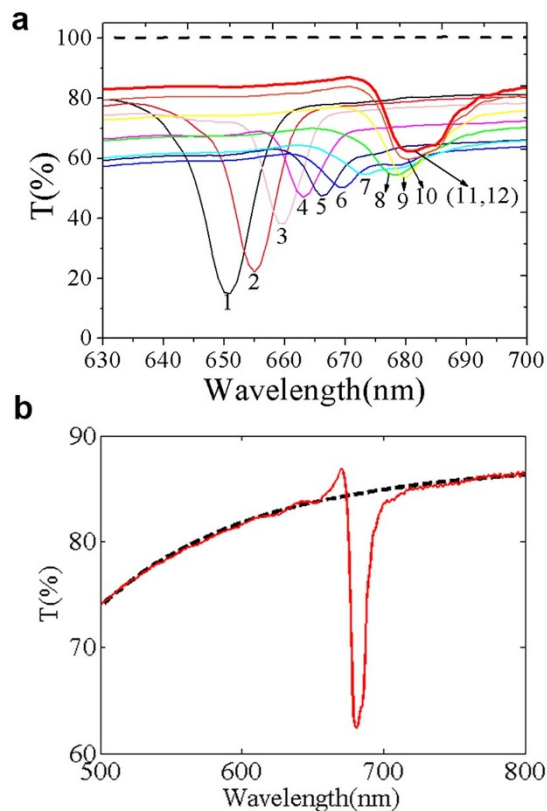an asymmetric band in spectrum would be expected.

**Figure 2 | PBG changes with time and exhibited an asymmetry profile of
asymmetry.** (a) PBGs changes with time at an interval of 90 s when they
continually adsorbed ethanol gas, dash line is transmittance spectrum of
saturated ethanol gas. And, asymmetric profile exists in the PBGs, such as
line 11 and 12 (b) shows a clearly asymmetry profile in which the short
wavelength photonic band edge is much higher than the long wavelength.
Dash line is the fitting curve without PBG.

Figure 2 shows the change of transmittance spectra of the as-pre-
pared sample with exposing time at an interval of 90 s to a saturated
ethanol gas at room temperature. With the increase of time for the
sample placed in the surrounding of saturated ethanol gas, the
adsorbed ethanol gas in the pores will gradually increase. It can be
seen from Figure 2a that the position of PBG has a red shift with the
increase of adsorbed ethanol gas in the pores of AAO; meanwhile,
transmittance at bottom of the band gap has an upward trend over
time. After 11 times measurement (about 16.5 minutes), the PC
reaches adsorption equilibrium which can be verified by the coin-
cidence of curves 11 and 12. It is noted that, light absorption of
ethanol has little impact on the PBG profile located in visible light
region, which is demonstrated by the transmittance spectrum of
saturated ethanol gas shown by the dash line in Figure 2a.

Furthermore, transmittance spectra (Figure 2a) exhibit asym-
metry profiles which should be drawn particular attention. It can
be seen that for curve 1, the photonic band edge (PBE) in short
wavelength side is relatively flat, and the PBE in long wavelength
side drops abruptly. However, for curves 11 and 12 the transmittance
spectrum shows different type of asymmetry profiles: The short
wavelength PBE drops abruptly while the long wavelength PBE is
relatively flat. By comparing the transmittance spectrum of curve 11
in Figure 2a with the fitting curve without PBG shown by Figure 2b,
this asymmetry can be seen clearly. Meanwhile, the short wavelength
PBE shows a dramatically increase. These results indicate that it has
characteristics of Fano resonance, so we think the exhibited asym-
metry profile of the PBGs results from resonance between the Bragg
scattering and CDTS.

Theoretical simulations. In order to understand the physical nature of asymmetry profile of PBGs, theoretical simulations were carried out. The effective dielectric constant of stem channel layer and branched channel layer can be given by the following Bruggeman formula[35]:

$$\sum_i f_i \left(\frac{\varepsilon_i - \varepsilon_{eff}}{\varepsilon_i + 2\varepsilon_{eff}} \right) = 0 \qquad (1)$$

where ε_i is dielectric constant of ith substance, f_i is the corresponding volume fraction, ε_{eff} is effective dielectric constant of the mixture.

The transmission (t_1) and reflection (r_1) parts of one period (layer I and layer II shown in Figure 1a) were first calculated based on finite element analysis method, in which strong light scattering by the porous structure and Bragg scattering were both taken into account. Then, the PBG profiles were analyzed using Transfer Matrix Method (TMM). The transfer matrix ($\widehat{M}_N$) of PC with N periods can be written as:

$$\widehat{M}_N = (\widehat{M}_1)^N = \begin{pmatrix} 1/t_N & r_N^*/t_N^* \\ r_N/t_N & 1/t_N^* \end{pmatrix} \qquad (2)$$

where $\widehat{M}_1$ is the transfer matrix of the sample within one period, t_N and r_N are the transmission and reflection part of PC with N periods, respectively. Superscript star (*) stands for conjugation of the corresponding terms. Herein, we have $|t_N|^2 + |r_N|^2 = T_N + R_N = 1$ for lossless medium, in which T_N and R_N are the transmittance and reflectance, respectively.

Simplified structure with a stem and a branched channel layer in one period as shown in Figure 1a is adopted in the simulations. The
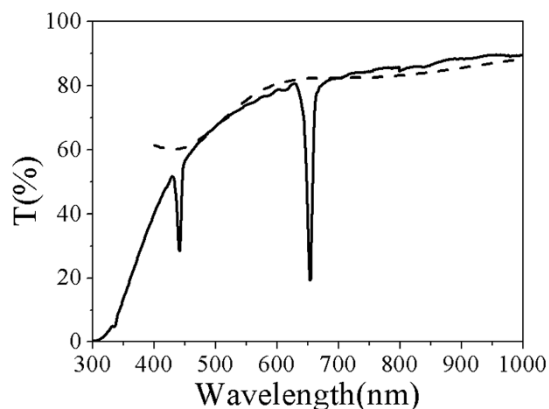

Figure 3 | Transmittance decrease from light scattering by the porous structure. Simulated transmittance decreases from light scattering by porous structure as the dash line shown compared with experimental one (solid line).

simulated thicknesses of layer I and layer II are 320 and 140 nm, respectively, and the corresponding pore diameters of these layers are 50 and 25 nm, respectively. The refractive indexes are $n_{\text{alumina}} = 1.7$, $n_{\text{air}} = 1$, $n_{\text{ethanol}} = 1.36$ for alumina, air and ethanol, respectively. Thus, the corresponding dielectric constants ($\varepsilon = n^2$) are $\varepsilon_{\text{alumina}} = 2.89$, $\varepsilon_{\text{air}} = 1$, $\varepsilon_{\text{ethanol}} = 1.85$, for alumina, air and ethanol, respectively. The simulation wavelength ranges from 300 to 1000 nm, and the period number is $N = 60$. In the simulations, strong light scatter-
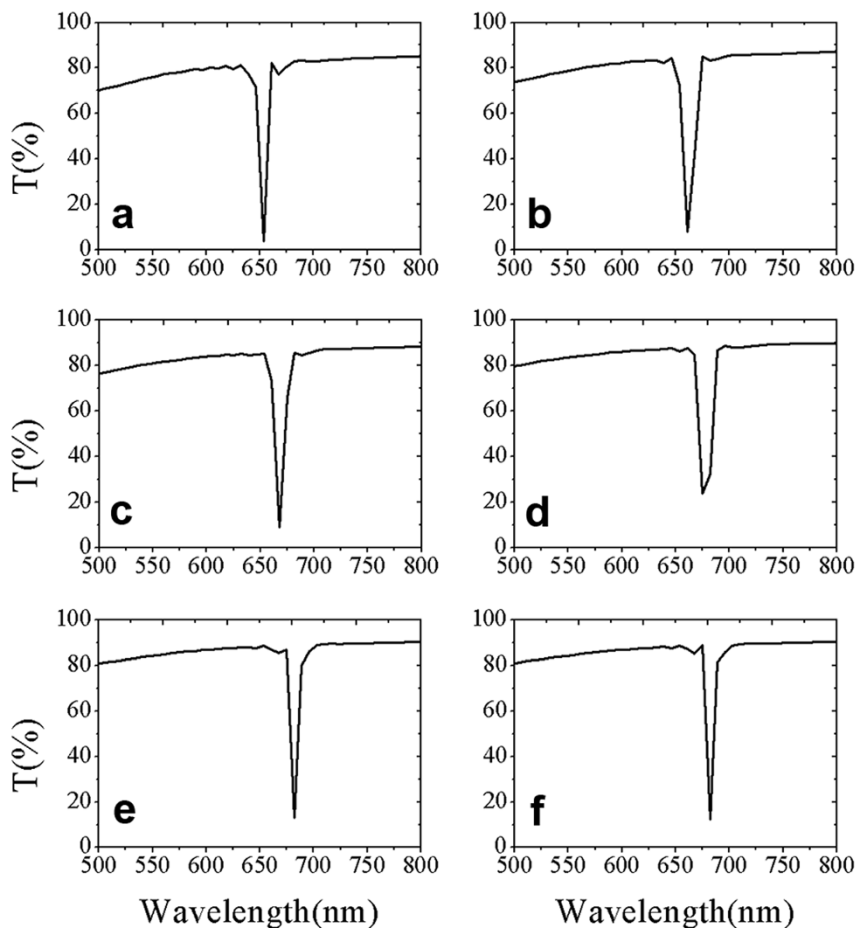

Figure 4 | Simulation results of the PBG at different wavelengths. Simulations show that the PBG exhibits a Fano type profile. Filling refractive indexes of the air pore for image (a–f) are 1.0000, 1.0600, 1.1030, 1.1575, 1.1740 and 1.1760, respectively.

ing by the porous structure and Bragg scattering are both taken into account.

Figure 3 shows the simulated spectrum only considering transmittance decrease by background light scattering without Bragg scattering in comparison with the experimental result. It can be seen that the simulated transmittance is generally consistent with experimental result when the wavelength is above 450 nm. However, when the wavelength is lower than 450 nm, the simulated transmittance starts to go up which is different from the experimental result. This difference is thought to be that alumina has light absorption when light wavelength is below 450 nm. Comparing the simulated and experimental spectra, the transmittance decrease with decreasing wavelength above wavelength 450 nm is mainly from light scattering by the porous structure. Transmittance spectrum of the as-prepared sample shows that porous AAO based PC not only exist as an effective-refractive-index material leading to the photonic bandgaps, but also generate a strong light scattering shown by the decrease of the transmittance with the decreasing wavelength.

Furthermore, we introduced the Bragg interference by alternated dielectric layers in simulations. Refractive indexes of the pores were chosen to be 1.0000, 1.0600, 1.1030, 1.1575, 1.1740 and 1.1760, respectively, and the results are shown in Figure 4. It can be seen that with the increase of refractive index of filler in the channels, the position of PBG has a red shift, in accordance with the experimental results. And the transmittance spectra show different asymmetry profiles when the fillers in the pores has different refractive index. When the filling refractive index in pores is 1.0000 for curve in Figure 4a, the PBE in short wavelength side is relatively flat and the PBE in long wavelength side drops abruptly; however, when the filling refractive index in pores is 1.1760 for curve in Figure 4f, the short wavelength PBE drops abruptly while the long wavelength PBE is relatively flat.

For better comparison, the simulated results and experimental ones are plotted in Figure 5, where figure 5a is for the sample of air-filled and figure 5b is for that of ethanol gas saturated. As we can see from the simulated spectrum, the PBG is located at 652 nm which is consistent with the experimental one of air-filled. Meanwhile, the short wavelength PBE was relatively flat, but the long wavelength PBE was drop abruptly. Figure 5b shows the simulated curve in Figure 4f and experimental curve 11 in Figure 2a. It can be seen that the simulated PBG located at 681 nm which consists with the experimental PBG with the equilibrium adsorption of saturated ethanol gas, of which the long wavelength PBE was relatively flat; however, the short wavelength PBE was drop abruptly. Comparing these simulations with the experiment results, we can attribute the asymmetry profile in our experiments to the interference of the Bragg scattering by periodically layered structure and strong scattering by porous structure, which is Fano resonance.

Fano asymmetry parameter. Generally, Fano resonance can be described by factor F(Ω)[1], which can be expressed by the following equation (Eq. 3):

$$F(\Omega) = \frac{(\Omega + q)^2}{\Omega^2 + 1} \qquad (3)$$

where q is Fano asymmetry parameter, which describes the degree of asymmetry, $\Omega = (\omega - \omega_o)/(\gamma/2)$ is dimensionless frequency, ω_o is a central frequency and γ is width of the narrow band, in our experiment we take the FWHM of PBG as value γ.

Figure 6a–f shows the fitting curves with Eq. 3 for the experimental transmittance spectra curves 1, 4, 6, 8, 9 and 11 in Figure 2a, respectively. Figure 6g is the relationship between asymmetry parameter q obtained from Figure 6a–f and exposing time. As we can see from Figure 6g, with time increase, adsorbed ethanol gas in the pores will gradually increase, the asymmetry parameter q changes from positive value to negative one. Meanwhile, the absolute value of q which
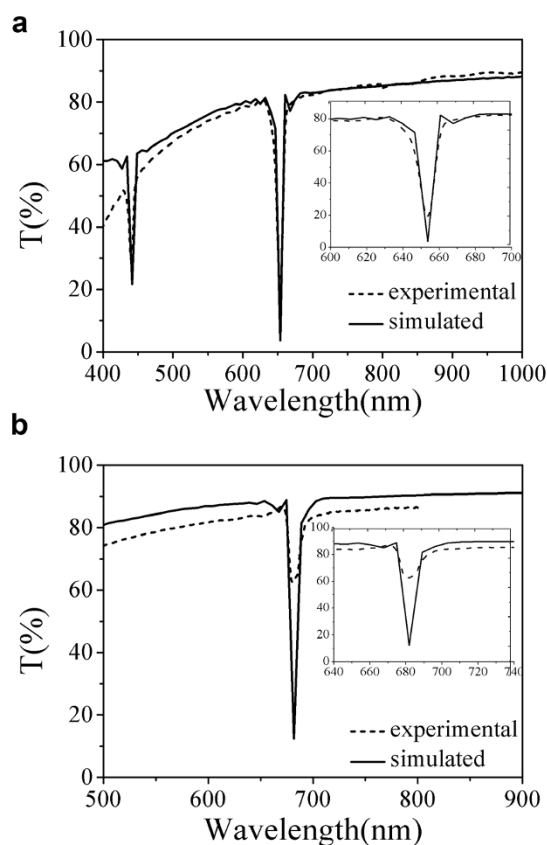

Figure 5 | Simulated results compared with the experimental one. Compare the simulation (solid lines) and experimental (dash lines) spectra when the as-prepared sample adsorbs no ethanol gas (a) and saturated ethanol gas (b), respectively. Inset is the corresponding enlarged spectrum.

means asymmetry strength of the profile is larger for curves 11 and 12 than that for curve 1. That is to say, the corresponding Fano resonance is stronger. This indicates that the absorbed ethanol gas in the pores affects Fano resonance intensity.

Discussion

Using compensation voltage mode, alumina PC with narrow PBG was prepared, which could avoid the bandgap profile asymmetry from the superposition of PBGs caused by structural inconsistencies. We found Fano resonance in the as-prepared alumina PC with narrow PBG, and this kind of resonance shows an asymmetric profile of the PBG. Transmittance spectra of the PC showed different asymmetry profiles with different asymmetry parameters by changing the effective refractive index of pores.

The Fano resonance could attribute to the interference between PBGs and background scattering. In the as-prepared samples there are two types of scattering states. One is Bragg scattering which can be regarded as a discrete state, and the other is the strong scattering revealed by decrease background of the transmittance which can be seen as a continuum state. Interference between the discrete state and the continuum state gives rise to a Fano resonance showing asymmetry profiles. According to the experimental results, we believe that the air-filled AAO based PC may have relatively small light scattering ability so that interference between this continuum light scattering and Bragg scattering is small. However, the exhibited Fano resonance is more clearly when the AAO based PC sufficiently absorbed saturated ethanol gas than air-filled AAO based PC. Since the transmittance of saturated ethanol gas almost keeps nearly 100% in visible light region (Figure 2a), we think that ethanol molecules has little impact on Fano resonance. Since there may exist capillary
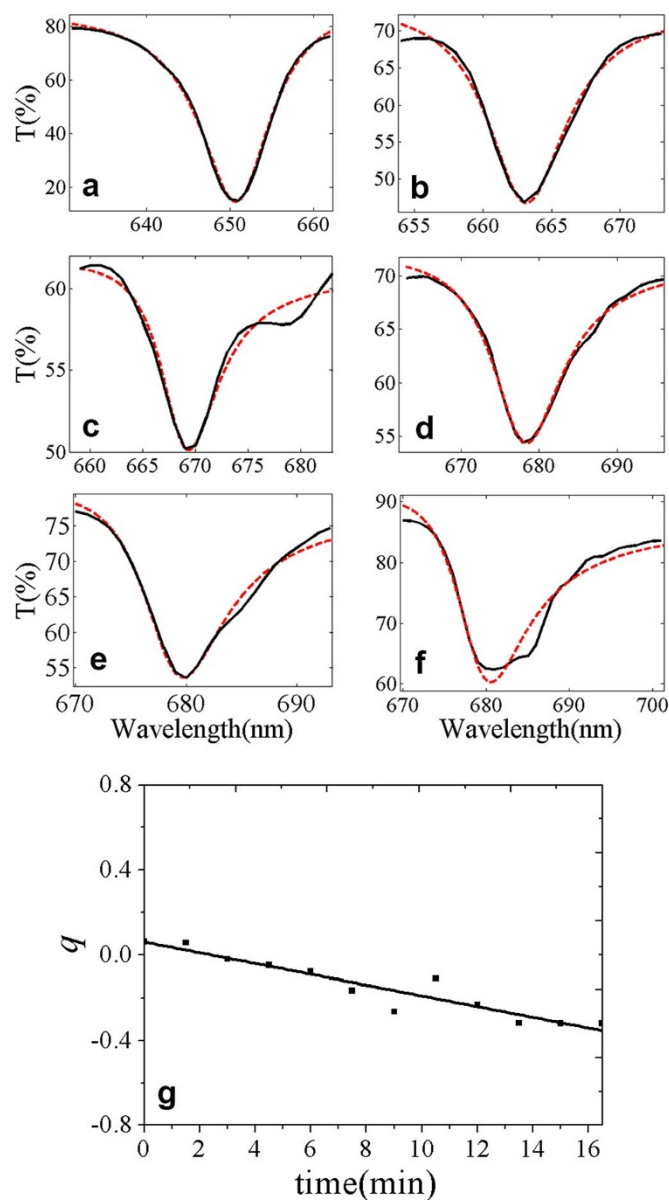
Figure 6 | Different Fano asymmetry parameter q for PBGs. Plots (a–f) are PBGs of curves 1, 4, 6, 8, 9 and 11 in Figure 2a, respectively, and the dash lines are fitting profiles based on Eq. 3 from which the corresponding Fano asymmetry parameter q is obtained. Figure 6g is parameter q change with time.

condensation of ethanol gas in the pores of AAO, light scattering would include scatterings both from porous structure and capillary condensed ethanol, which should be stronger than light scattering of air-filled PC. So, the interference between this continuum light scattering and Bragg scattering will be stronger and more clearly when the AAO was saturated ethanol gas.

In conclusion, we demonstrated a viable simple method to induce and analyze the Fano resonance in the AAO based PC. These findings could be applied in the fields of design and preparation of PCs with better performance, and some situations in which interaction between photonic bandgaps and scatterings from other factors is not negligible. In addition, using interactions of different scattering states in photonic crystals will provide a possible approach to fine adjustment of band gap structure.

Methods

Synthesis the narrow PBG. In our experiment, a two-step oxidation process was used to fabricate the AAO based PC. The pre-treatment and the first oxidation of the AAO

template were performed following the method description in our previous papers[33,34]. In detail, high-purity aluminum foils (99.999%) were first degreased in acetone and ethanol, then annealed at 500°C under vacuum ambient (about 2×10^{-5} Torr) for 5 h. After that, the aluminum foils were electro-polished in a 1 : 9 volume mixture of $HClO_4$ and C_2H_5OH for about 3 min. The first oxidation was carried out at a constant voltage of 53 V in 0.3 M/L $H_2C_2O_4$ for 3 h in ice water bath, then the formed alumina layer was removed by a mixed solution of 6 wt.% phosphoric acid and 1.5 wt.% chromic acid at 60°C. During the second oxidation, the compensation voltage mode was adopted[33]. In detail, in the first period of the voltage waveform, the voltage increased from V_L (=23 V) to V_H (=53 V) by a quarter of sinusoidal wave within $t = 30$ s and then linearly decreased to V_L from V_H within $t = 3$ min. From the second period, a compensation voltage was introduced. The voltage value of each period is overall higher than the previous one with a constant voltage of 0.055 V. All the second oxidations were controlled by computer and carried out in a water tank with constant temperature of 16°C.

Fano resonance characterization. After the sample was prepared, the PC was fixed in sealed quartz cuvette with enough liquid ethanol to produce a saturated ethanol gas circumstance. After 30 s delay, the transmittance spectrum in wavelength between 400 nm and 800 nm was recorded repeatedly. The two adjacent transmittance spectra have a 90 s measurement time interval.

Characterization. The morphologies of the samples were observed by a Field Emission Scanning Electron microscopy (FE-SEM, Sirion 200), and the transmittance spectra were measured by spectrophotometer (CARY 5E) with incident light perpendicular to the sample surface.

1. Fano, U. Effects of configuration interaction on intensities and phase shifts. *Phys. Rev.* **124**, 1866–& (1961).
2. Wickenhauser, M., Burgdorfer, J., Krausz, F. & Drescher, M. Time resolved Fano resonances. *Phys. Rev. Lett.* **94**, 023002 (2005).
3. Joe, Y. S., Satanin, A. M. & Kim, C. S. Classical analogy of Fano resonances. *Phys. Scr.* **74**, 259–266 (2006).
4. Kroner, M. *et al.* The nonlinear Fano effect. *Nature* **451**, 311–314 (2008).
5. Miroshnichenko, A. E., Flach, S. & Kivshar, Y. S. Fano resonances in nanoscale structures. *Rev. Mod. Phys.* **82**, 2257–2298 (2010).
6. Frimmer, M., Coenen, T. & Koenderink, A. F. Signature of a Fano resonance in a plasmonic metamolecule's local density of optical states. *Phys. Rev. Lett.* **108**, 077404 (2012).
7. Bachelier, G. *et al.* Fano profiles induced by near-field coupling in heterogeneous dimers of gold and silver nanoparticles. *Phys. Rev. Lett.* **101**, 197401 (2008).
8. Ridolfo, A., Di Stefano, O., Fina, N., Saija, R. & Savasta, S. Quantum plasmonics with quantum dot-metal nanoparticle molecules: Influence of the Fano effect on photon statistics. *Phys. Rev. Lett.* **105**, 263601 (2010).
9. Francescato, Y., Giannini, V. & Maier, S. A. Plasmonic Systems Unveiled by Fano Resonances. *ACS nano* **2012**, 6, 1830–1838.
10. Luk'yanchuk, B. *et al.* The Fano resonance in plasmonic nanostructures and metamaterials. *Nat. Mater.* **9**, 707–715 (2010).
11. Fu, Y. H., Zhang, J. B., Yu, Y. F. & Luk'yanchuk, B. Generating and manipulating higher order Fano resonances in dual-disk ring plasmonic nanostructures. *ACS nano* **6**, 5130–5137 (2012).
12. Wu, C. *et al.* Fano-resonant asymmetric metamaterials for ultrasensitive spectroscopy and identification of molecular monolayers. *Nat. Mater.* **11**, 69–75 (2012).
13. Yablonovitch, E. Inhibited spontaneous emission in solid-state physics and electronics. *Phys. Rev. Lett.* **58**, 2059–2062 (1987).
14. John, S. Strong localization of photons in certain disordered dielectric superlattices. *Phys. Rev. Lett.* **58**, 2486–2489 (1987).
15. Steinvurzel, P., Martijn de Sterke, C., Steel, M. J., Kuhlmey, B. T. & Eggleton, B. J. Single scatter Fano resonances in solid core photonic band gap fibers. *Opt. Express* **14**, 8797–8811 (2006).
16. Grillet, C. *et al.* Characterization and modeling of Fano resonances in chalcogenide photonic crystal membranes. *Opt. Express* **14**, 369–376 (2006).
17. Song, J. F., Zaccaria, R. P., Yu, M. B. & Sun, X. W. Tunable Fano resonance in photonic crystal slabs. *Opt. Express* **14**, 8812–8826 (2006).
18. Ricciardi, A. *et al.* Guided resonances in photonic quasicrystals. *Opt. Express* **17**, 6335–6346 (2009).
19. Galli, M. *et al.* Light scattering and Fano resonances in high-Q photonic crystal nanocavities. *Appl. Phys. Lett.* **94**, 071101 (2009).
20. Chua, S. L., Chong, Y. D., Stone, A. D., Soljacic, M. & Abad, J. B. Low-threshold lasing action in photonic crystal slabs enabled by Fano resonances. *Opt. Express* **19**, 1539–1562 (2011).
21. Chen, W. J., Lee, J. C. W., Dong, J. W., Qiu, C. W. & Wang, H. Z. Fano resonance of three-dimensional spiral photonic crystals: Paradoxical transmission and polarization gap. *Appl. Phys. Lett.* **98**, 081116 (2011).
22. Zhang, Y. B., Hu, X. Y., Fu, Y. L., Yang, H. & Gong, Q. H. Ultrafast all-optical tunable Fano resonance in nonlinear ferroelectric photonic crystals. *Appl. Phys. Lett.* **100**, 031106 (2012).
23. Zanotto, S., Degl'Innocenti, R., Sorba, L. & Tredicucci, A. Analysis of line shapes and strong coupling with intersubband transitions in one-dimensional metallodielectric photonic crystal slabs. *Phys. Rev. B* **85**, 035307 (2012).

24. Rybin, M. V. *et al.* Fano resonance between Mie and Bragg scattering in photonic crystals. *Phys. Rev. Lett.* **103**, 023901 (2009).

25. Poddubny, A. N., Rybin, M. V., Limonov, M. F. & Kivshar, Y. S. Fano interference governs wave transport in disordered systems. *Nat. Commun.* **3**, 914 (2012).

26. Soboleva, I. V., Moskalenko, V. V. & Fedyanin, A. A. Giant Goos-Hanchen effect and Fano resonance at photonic crystal surfaces. *Phys. Rev. Lett.* **108**, 123901 (2012).

27. Nojima, S., Usuki, M., Yawata, M. & Nakahata, M. Fano resonances for localized intrinsic defects in finite-sized photonic crystals. *Phys. Rev. A* **85**, 063818 (2012).

28. Babic, L. & de Dood, M. J. A. Interpretation of Fano lineshape reversal in the reflectivity spectra of photonic crystal slabs. *Opt. Express* **18**, 26569–26582 (2010).

29. Wang, B., Fei, G. T., Wang, M., Kong, M. G. & Zhang, L. D. Preparation of photonic crystals made of air pores in anodic alumina. *Nanotechnology* **18**, 365601 (2007).

30. Zheng, W. J., Fei, G. T., Wang, B. & Zhang, L. D. Modulation of transmission spectra of anodized alumina membrane distributed Bragg reflector by controlling anodization temperature. *Nanoscale Res. Lett.* **4**, 665–667 (2009).

31. Su, Y. *et al.* Anodic alumina photonic crystal heterostructures. *J. Opt. Soc. Am. B* **28**, 2931–2933 (2011).

32. Yan, P. *et al.* Anti-counterfeiting of one-dimensional alumina photonic crystal by creating defects. *Electrochem. Solid St.* **15**, K23–K26 (2012).

33. Shang, G. L. *et al.* Preparation of narrow photonic bandgaps located in near infrared region and their applications on ethanol gas sensing. *J. Mater. Chem. C* **1**, 5285–5291 (2013).

34. Shang, G. L. *et al.* Preparation of the very uniform pore diameter of anodic alumina oxidation by voltage compensation mode. *Mater. Lett.* **110**, 156–159 (2013).

35. Choy, T. C. *Effective Medium Theory: Principles and applications* (Oxford University Press, 1999).

Author contributions

G.T.F. and G.L.S. designed the experiments. G.L.S. and Y.Z. conducted simulations. G.L.S., G.T.F. and Y.Z. analysed data. G.T.F., G.L.S., Y.Z., P.Y., S.H.X., H.M.O. and L.D.Z. discussed the results and contributed to the writing of the manuscript.

Additional information

Competing financial interests: The authors declare no competing financial interests.

How to cite this article: Shang, G.L. *et al.* Fano resonance in anodic aluminum oxide based photonic crystals. *Sci. Rep.* **4**, 3601; DOI:10.1038/srep03601 (2014).